# Simulation of Dye-Sensitised Solar Cell with Mesoporous Zinc Oxide Layer of Different Thicknesses and with Dye-Sensitisers of Different Absorption Coefficients

Lavanyah Arumugam, Pei Ling Low[✉], Mian En Yeoh, Gregory Thien, Yew Keong Sin, and Kah Yoong Chan

Faculty of Engineering, Multimedia University, Cyberjaya, Malaysia
lavanyah2104@gmail.com, pllow@mmu.edu.my

**Abstract.** Dye-sensitised solar cells (DSSCs) are an important part of research on renewable energy sources as they are less complicated to manufacture and cost less than several other types of solar cells. The performance of DSSC with a combination of mesoporous zinc oxide and natural dyes are simulated using COMSOL Multiphysics. Numerical expression of the electrical properties of a dye-sensitised solar cell is applied to a two-dimensional structure to form an electrical model. Optical properties of the natural dyes are then coupled with this electrical model. The variables tested are thickness of the photoanode layer and absorption coefficient of dyes. Efficiency of the simulated zinc oxide solar cell with N719 dye is 12.4%. Maximum power of 0.309 µW is obtained at a photoanode thickness of 600 nm with current density of 16.815 mA/cm$^2$ and voltage of 0.756 V. The natural dyes simulated are chlorophyll, betalain and anthocyanin. Of the three, the one with the highest absorption coefficient i.e., betalain resulted in the highest efficiency solar cell. The results were more favourable than several simulations studying titanium dioxide based DSSC.

**Keywords:** Dye-sensitised solar cell · Simulation · Power conversion efficiency · J-V plot

## 1 Introduction

Solar cells promise the realisation of clean energy plans due to their ability to convert renewable solar energy into electrical energy. Dye-sensitised solar cell (DSSC) is a type of hybrid solar cell that has good performance even under low light conditions [1]. It was first invented by Professor Graetzel to achieve efficiencies beyond that of silicon solar cells. They can be manufactured cleanly as the fabrication process is low-temperature and is flexible with the use of substrates [2]. Silicon conductors still have one of the highest efficiencies [3], however, moving towards an era of sustainability, it is imperative to further study and enhance the DSSC through research.

DSSCs with mesoporous semiconductors are researched because of better dye loading, electron transport and light harvesting compared to non-mesoporous structures.

Mesoporous materials are also known as super-nanoporous, or containing pores with diameters between 2 nm and 50 nm [4].

DSSCs are largely manufactured commercially using titanium dioxide, $TiO_2$ as the semiconductor in the photoanode layer and a ruthenium (Ru) complex dye known as N719. Firstly, radiation from the visible light spectrum is poorly absorbed by $TiO_2$ [2]. Additionally, DSSCs with $TiO_2$ based photoanodes have their efficiency limited by the recombination of excited electrons from the dye with the electrolyte, contributing to dark current. Zinc oxide (ZnO) nanoparticles are capable of reducing recombination problem due to having a direct electron flow path which results in greater electron mobility and lifetime [3]. Moreover, research on other dyes is imperative since Ru complexes are expensive and not easy to synthesise [2]. Although natural dyes are less efficient [5], they are readily available, cheap, biodegradable and non-toxic [3].

In accordance with those justifications, studying a DSSC with ZnO-based photoanode and natural dye is significant for the advancement of nanostructured solar cell technology. In this work, electrical performance of a DSSC is studied through simulation of an analytical model by varying photoanode thickness and absorption coefficient of natural dye-sensitisers. A photoanode layer of mesoporous ZnO nanoparticles with N719 synthetic dye is modelled. The N719 dye is compared with three of the most efficient natural dyes, which are chlorophyll, betalain and anthocyanin. Optimum photoanode thickness for a mesoporous ZnO DSSC and a suitable natural dye-sensitiser is proposed.

## 2   Literature Review

A DSSC is made up of transparent conductive oxide (TCO) electrode, photoanode layer, electrolyte and counter-electrode. The photoanode layer consists of semiconducting metal oxide adsorbed with dye-sensitiser. Figure 1 shows the structure of a titanium dioxide ($TiO_2$) DSSC [1]. Electron generation occurs in the photoanode. The TCO electrode collects and transports photoexcited electrons to the external circuit through quantum confinement of charge carriers [6].

A dye is diffused into the mesoporous metal oxide layer to photosensitise it. The dye molecules generate photoexcited free electrons which are injected to the conduction band of the semiconductor metal oxide [1][7]. The excited electrons diffuse from the metal oxide to the surface of the TCO [7] where they do work on the load in an external circuit before reaching the counter-electrode.

An electrolyte with suitable redox potential separates the photoanode from the counter electrode. When a ground-state electron from the dye is photoexcited and leaves,
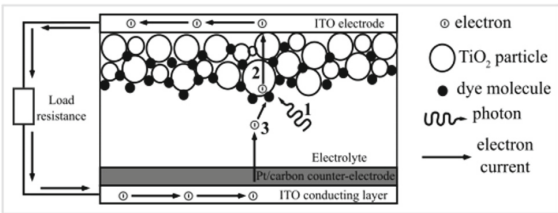


**Fig. 1.**  DSSC structure and working principle [1].

the dye is oxidised [7]. The electrolyte then donates an electron to restore the dye configuration, which oxidises the electrolyte, while electrons at the counter-electrode reduces the electrolyte [3]. This cyclic process results in the DSSC having a high power conversion efficiency (PCE). Performance of the DSSC depends on the rate of photogeneration, electron transportation and recombination rate.

Commercially, $TiO_2$ is most extensively used for the metal oxide layer, while ZnO-based DSSC has also gained traction as a competitor [3]. Doping of the photoanode layer is sometimes done to increase charge production or alter band energies to reduce mismatch between layers. Other than metal oxides, cadmium selenide (CdSe) and titanium nitride (TiN) are also used as photoanodes [8]. Photoanode layer are sensitised with synthetic dyes such as N719, N3, Z907, Y123 [9] and zinc porphyrin [10], or natural pigments such as chlorophyll, betalain, anthocyanin [11], carotenoid and flavonoids [2].

## 2.1 Influence of Design Parameters on DSSC Performance

Photocurrent and photovoltage are limited by the number of photogenerated electrons as well as the number of electrons that actually contribute to the output [7]. Thus, properties of the photoanode layer must be optimally designed since this is where photogeneration and recombination primarily occurs. Examples of design parameters include electron diffusion coefficient [1], doping, bandgap energy of material used for the photoanode layer [8], surface area to volume ratio of different shapes and sizes of nanoparticles [6][17–19], spectral response to light and diffusivity or adhesion of dye to metal oxide [8]. The following subsections discuss specifically about the influence of thickness of the photoanode layer and dye-sensitiser used as those are the main focus of this report.

### 2.1.1 Photoanode Thickness

In order to gather as much solar energy as possible, a thicker photoanode is preferred as high interfacial surface area between the dye and metal oxide increases electron injection and PCE per unit area of the DSSC [15]. Nevertheless, chances of charge recombination are significantly higher for thicker photoanodes. This is because the distance required to be travelled by electrons will be much greater than the diffusion length. In DSSCs, electrons are prone to recombine with the dye before reaching the electrode on the other end of the metal oxide layer [8]. As a result, conversion efficiency from solar energy to electrical energy is low because injected electrons are lost. Moreover, the series resistance of the solar cell is greater, further reducing its open-circuit voltage and efficiency [6].

Conversely, a thinner photoanode layer allows more light to easily penetrate its entire depth, making use of all available dye-adsorbed metal oxide particles, besides having a lower recombination rate. However, free electron diffusion cannot properly occur at too small thicknesses, causing a loss of solar power [1].

### 2.1.2 Types of Dyes

Among the dye properties to consider are absorption coefficient and anchoring ability [11]. High absorption coefficient of dye means more light energy able to be absorbed per unit mass or thickness of the photoanode layer [12]. Plus, dyes with carbonyl or
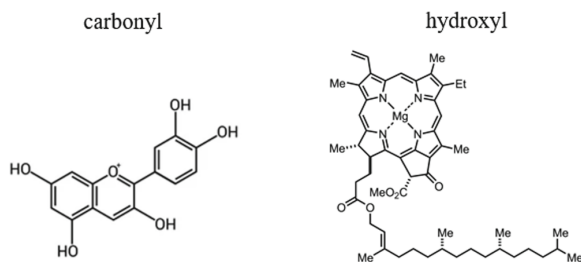
**Fig. 2.** Carbonyl (C = O) and hydroxyl (C-O-H) group found in molecular structures of anthocyanin and chlorophyll dyes, respectively [3].

hydroxyl group are observed to attach well to metal oxide layers. Figure 2 shows two natural dyes having functional groups with anchoring ability [3]. Besides that, wider absorption spectrum of dye particles results in more wavelengths of sunlight harvested, increasing rate of photogeneration [8]. Dye compatibility is also important. For example, the acidic nature of N719 dye causes aggregation of dye to form in ZnO, leading to poor dye adsorption and hindering of electron injection [16]. The ZnO layer breaks down over time and forms $Zn^{2+}$ ions. This phenomenon also occurs with indoline ($C_8H_9N$) dyes.

Synthetic dyes are known to be more efficient than natural dyes because of their low recombination tendency of charges. However, they are expensive and difficult to synthesise [2]. Natural dyes are cheap [5], easily available, completely biodegradable [12] and highly absorbent of UV light or infrared (IR) rays which compose a large range in the solar spectrum [3]. High efficiency natural dyes include chlorophyll, carotenoid, flavonoid and anthocyanin – chlorophyll especially so since it naturally absorbs ultra-violet (UV) and visible light [2]. Even so, natural dyes have lower efficiency compared to synthetic dyes as they have weak spectral response and are slightly unstable in the visible light spectrum. Efficiency of natural dye DSSCs can be increased by doping the metal oxide layer to shift and match its absorption spectrum with the dye.

## 2.2 Works on Fabricated DSSC

In the lab, oxide layer of DSSCs can be deposited on a substrate by deploying simple methods such as brush painting, doctor blading, spin coating [2], hydrothermal sol-gel, flame spray pyrolysis [5] and chemical bath deposition [3]. Natural dyes are obtained by crushing or pounding plant parts such as leaves, flowers and roots in alcohol or ketone solvents [2][5]. A substrate with metal oxide layer deposition is usually immersed into the dye extract for some time to facilitate adsorption [2].

### 2.2.1 Effects of Photoanode Thickness

Studies on the effect of photoanode thickness found that performance of DSSC was weak at smaller thicknesses. Electron injection was delayed, and quantum confinement caused a shift in the bottom conduction band towards vacuum [9]. As thickness is increased, short-circuit current, $J_{SC}$ and efficiency, $\eta$ increases due to higher surface area being

available for dye adsorption [9][13][17]. Both parameters peak at an optimum thickness near which maximum output power is achieved [2]. Beyond the optimum thickness, values of the parameters declined as injected electrons become lost to more traps since transport distance is longer. Series resistance along the DSSC stack also increases, slightly reducing open-circuit voltage, $V_{OC}$ [15][17].

### 2.2.2 Effects of Types of Dyes

Fabricated DSSCs using different types of dyes resulted in greatest $\eta$ and output power for the dye with the highest absorbance or absorption coefficient [8][11][12]. When two dyes of low absorbances are mixed, they add up and further increase overall efficiency because light can be absorbed across a wider spectrum of solar power [3]. Dyes with high absorption coefficient absorb more photons instead of letting them pass through. Transmittance decreases exponentially with increasing absorbance [11]. Generally, synthetic dyes have higher absorbances. However, photogeneration capabilities of beetroot dye was managed to be improved beyond that of N719 dye by doping $TiO_2$ in the photoanode with silver vanadium trioxide ($AgVO_3$). Doping contributed to photon absorption in the UV region while the beetroot dye absorbed photons from visible light of the solar spectrum. Due to the wider range of solar spectrum absorbed, $\eta$ improved [18].

### 2.3 Works on Simulated DSSC

Frequently used software for simulation or modelling of DSSCs are MATLAB and SILVACO Atlas TCAD, which are common in semiconductor related research. DSSC simulations are performed under steady-state conditions or thermal equilibrium. One of the assumptions made in the simulations is absence of internal electric field within the photoanode. Therefore, photogenerated electrons are not transported through drift, but only through diffusion [1][5].

In equilibrium, generation, transportation and recombination of electrons is as represented by Eq. (1). It is a function of the absorption coefficient, $\alpha$, diffusion coefficient, $D_0$, incident irradiation intensity, $\varnothing$, electron lifetime, $\tau_0$ and dark electron concentration, $n_0$ [5][10][27–29]. $n(x)$ is free electron concentration in the photoanode layer and $x$ is position perpendicular to the surface area of the DSSC stack.

$$D_0 \frac{\partial^2 n(x)}{\partial x^2} - \frac{n(x) - n_0}{\tau_0} + \varnothing \alpha exp(-\alpha x) = 0 \qquad (1)$$

Equations (2) and (3) also sum up photogeneration and recombination of electrons without using absorption coefficient. Instead, optical property of the DSSC is included in the photoexcited electron generation rate, $G_e$, described in Eq. (4) as an integral across the solar spectrum. It is a function of imaginary component of permittivity of metal oxide, $\varepsilon''$ [22]. $L$ is electron diffusion length, $n_{CB}$ is conduction band electron density, $\lambda$ is wavelength of incident light, $h$ is Planck's constant, $E$ is electric field and $\pi$ is the constant.

$$L^2 \nabla^2 n_{CB} - (n_{CB} - n_0) + \tau_0 G_e = 0 \qquad (2)$$

$$L = \sqrt{D_0 \tau_0} \qquad (3)$$

$$G_e = \int_\lambda \frac{\varepsilon'' |E|^2 \pi}{h} d\lambda \qquad (4)$$

Another way is using Fick's first law of diffusion, depicted in Eq. (5), to represent current density. The differential term represents the one-dimensional diffusion profile of electron concentration [1]. $J_{diff}$ is diffusion current density and $e$ is electron charge.

$$J_{diff} = -eD_0 \frac{\partial n}{\partial x} \qquad (5)$$

Other than that, 1D Schrödinger equation can be used to solve for wave functions of every electron and hole of the DSSC. By applying Fermi-Dirac statistics which dictate that each discrete state can only be occupied by one particle, electron concentration in the conduction band can be expressed. Using this information, electric potential of the DSSC can be determined by solving Poisson's equation [23].

### 2.3.1 Effects of Photoanode Thickness

Works on effects of photoanode thickness in simulated DSSCs mainly focus on $TiO_2$. The outcome conforms to those of fabricated DSSCs, except that the computed efficiency is much higher. However, overall efficiency is still less than 5%. Very thin photoanode layer yielded $\eta$ lower than 1.5% because free electron diffusion is unable to take place properly [1].

Photocurrent density increased with increasing thickness because more photons could be absorbed by the photoanode [19]. Larger contact surface between dye-sensitiser and metal oxide boosts electron injection rate [20]. When thickness is increased further than optimum value, photocurrent density decreased since electron recombination rate is greater [19][20]. Furthermore, electron back transfer to the electrolyte contributes to lower $V_{OC}$ at greater thicknesses [19]. Efficiency was highest at the optimum thickness.

### 2.3.2 Effects of Types of Dyes

Effects of dye types on DSSC performance is mainly focused on the absorption coefficient of dye-sensitisers. Dyes with higher absorption coefficient proved better photogeneration capabilities and electrical performance [5][20][24][25]. Performance parameters were higher for dye with wider absorption spectra and absorbance as more wavelengths of light can be absorbed [10].

## 3   Methodology

COMSOL Multiphysics is used to design the analytical model of DSSC. It is a simulation software employing finite element method (FEM) that allows conventional physics-based user interfaces and coupled systems of partial differential equations. It is used to simulate various complex systems such as microfluidics, particle tracing and biomechanics among
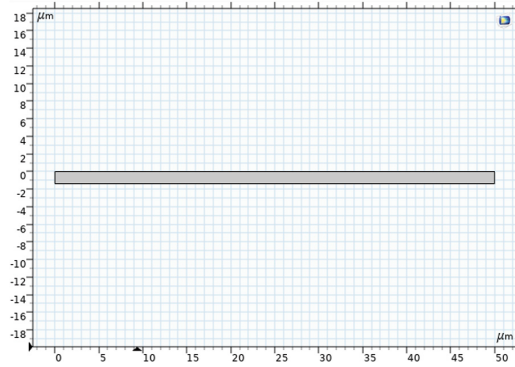
**Fig. 3.** Rectangular geometry of the photoanode layer having a width of 50 μm and thickness of $d = 1400$ nm.

many others due to its flexibility of design parameters. However, few research employ it for electronics, and fewer still for DSSC simulation.

The model designed only consists of the photoanode layer of the DSSC as it is the main site of action for the manipulated variables. Dynamics of the interaction between the photoanode layer with the TCO, electrolyte and external circuit is omitted to reduce complexity and to analyse the outcomes with scrutiny. The assumptions made in the designing of this model are as follows:

1. The DSSC is in steady-state condition or thermal equilibrium.
2. Current only through diffusion and not drift.
3. Solar ray is incident at an angle of 90° on the surface area of the DSSC.
4. No reverse saturation current present in the DSSC.
5. The dye completely adsorbs into entire thickness of ZnO layer.

To construct the model, first Coefficient Form Partial Differential Equation (PDE) module is chosen with stationary study type. Then, a two-dimensional photoanode layer with a surface area, $A$ of 50 μm × 50 μm is built as shown in Fig. 3 and assigned with ZnO nanoparticles as material. The top horizontal edge is the photoanode-TCO boundary while the bottom horizontal edge is the photoanode-electrolyte boundary.

The geometry was meshed with an extremely fine physics-controlled mesh as shown in Fig. 4 to compute the solution accurately. Then, an optical model and electrical model were designed with the absorption coefficient of the photoanode layer, $\alpha$ and incident irradiation intensity, $\Phi_0$ as the link between both.

The thickness of the photoanode, $d$ was varied from 200 nm to 3000 nm. Optimum thickness was determined from the resulting performance parameters to be used for the study on absorption coefficient of natural dye-sensitisers, chlorophyll, betalain and anthocyanin. From the electrical performance of the DSSC, an optimum range of thickness and suitable natural dye was suggested for mesoporous ZnO-based DSSC.
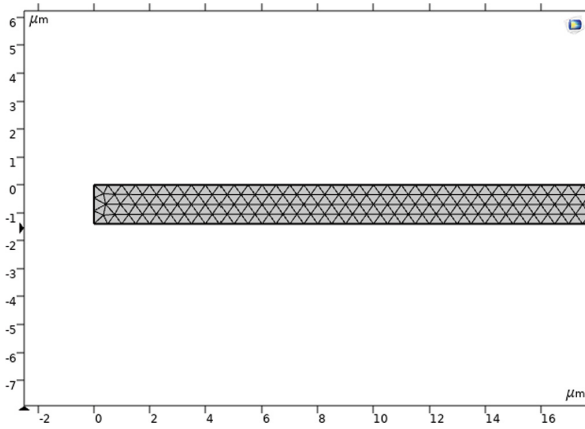
**Fig. 4.** Meshed and zoomed-in geometry of DSSC.

## 3.1 Optical Model

Extinction coefficient, $k$ i.e., the complex part of refractive index is used to determine $\alpha$, in Eq. (6) [6].

$$\alpha = \frac{4\pi k}{\lambda} \tag{6}$$

Absorption coefficient of ZnO and dye-sensitiser composite was determined using Beer-Lambert law, that is, if more than one species absorb at the same wavelength without chemically interacting with each other, the total absorbance, $A_{total}$ is the sum of the individual absorbances for each species [26]. Equation (7) below describes this relationship.

$$A_{total} = A_1 + A_2 \tag{7}$$

Relationship between $A$ and $\alpha$ is shown in Eq. (8).

$$A = \log e \times d \times \alpha \tag{8}$$

Assuming the dye has sensitised the entire thickness of ZnO, $\log e$ and $d$ become constants. Therefore, the total absorption coefficient of the dye and ZnO composite is the sum of the individual absorption coefficients as described by Eq. (9), where $\alpha_1$ and $\alpha_2$ are absorption coefficients of dye and ZnO, respectively.

$$\alpha = \alpha_1 + \alpha_2 \tag{9}$$

Using the thickness of DSSC yielding the highest efficiency, $\alpha_1$ was changed according to those of the types of dyes studied. Maximum values of $\alpha_1$ were input into the simulation regardless of which wavelength they occur at since the absorbance spectrum overlaps across frequencies. Another parameter that links the optical model and electrical model is the incident irradiation intensity, $\Phi_0$ which is equal to $1 \times 10^{17}$ cm$^{-2}$s$^{-1}$.

### 3.2 Electrical Model

Equation (10) is used to represent transportation, recombination and generation of electrons in the photoanode layer [5][10][19][20][21]. $D_0$ is diffusion coefficient, $n(x)$ is free electron concentration in the photoanode layer, $x$ is position perpendicular to the surface area of the DSSC, $n_0$ is dark electron concentration, $\tau_0$ is electron lifetime, $\Phi_0$ is incident irradiation intensity and $\alpha$ is absorption coefficient of the photoanode layer.

$$\underbrace{D_0 \frac{\partial^2 n(x)}{\partial x^2}}_{\text{carrier diffusion}} - \underbrace{\frac{n(x)-n_0}{\tau_0}}_{\text{bulk recombination}} + \underbrace{\Phi_0 \alpha exp(-\alpha x)}_{\text{generation}} = \underbrace{\frac{\partial n}{\partial t}}_{\text{excess carrier concentration}} \tag{10}$$

Under steady-state condition, the Eq. (10) becomes Eq. (11).

$$D_0 \frac{\partial^2 n(x)}{\partial x^2} - \frac{n(x) - n_0}{\tau_0} + \Phi_0 \alpha exp(-\alpha x) = 0 \tag{11}$$

A Dirichlet boundary condition was placed at the photoanode-TCO interface, equating the free electron density to the dark electron concentration as shown in Eq. (12) [5][20][22].

$$n(0) = n_0 \tag{12}$$

Equation (13) describes a Neumann boundary condition placed at the photoanode-electrolyte interface using the flux/source node [5][20][22].

$$\left(\frac{dn}{dx}\right)_{x=d} = 0 \tag{13}$$

Periodic boundary condition is applied along either side of the geometry which guides the solution to free electron concentration, $n$ to be equal at every horizontal slice of the geometry.

Output current density, $J$ and voltage, $V$ are obtained from Eq. (14) and Eq. (15), respectively [5][10][19][20].

$$J = \frac{e\emptyset L\alpha}{1 - L^2\alpha^2} \left[ \frac{-L\alpha + tanh\left(\frac{d}{L}\right) + L\alpha e^{-d\alpha}}{cosh\left(\frac{d}{L}\right)} \right] \tag{14}$$

$$V = \frac{k_B T \gamma}{e} ln \left[ \frac{L(J_{sc})}{eD_0 n_0 tanh\left(\frac{d}{L}\right)} + 1 \right] \tag{15}$$

Table 1 shows the parameter values used in the simulation for ZnO nanoparticles.

$J$ against $V$ graph was plotted, and performance parameters were calculated as expressed by Eq. (16) to Eq. (20) [3][6]. In Eq. (17), $J_{SC}$ is the current density when the output voltage, $V$ is zero. $V_{OC}$ is voltage when current density, $J$ is zero.

$$P_{max} = J_{maxp} \times V_{maxp} \times A \tag{16}$$

**Table 1.** Table of parameter values used in the simulation

| Parameter | Value | Reference(s) |
|---|---|---|
| Surface area of DSSC, $A$ | $2.5 \times 10^{-9}$ m$^2$ | |
| Diffusion coefficient, $D_0$ | $1.7 \times 10^{-4}$ cm$^2$s$^{-1}$ | [27][28] |
| Electron lifetime, $\tau_0$ | 0.0252 s | [14] |
| Electron diffusion length, $L$ | 20.6978 μm | [14] |
| Dark electron concentration, $n_0$ | $1 \times 10^{16}$ cm$^{-3}$ | [21] |
| Absolute temperature, $T$ | 293.15 K | |
| Ideality factor, $\gamma$ | 3.07 | [29] |
| Incident irradiation intensity, $\Phi_0$ | $1 \times 10^{17}$ cm$^{-2}$ s$^{-1}$ | [23] |

$$FF = \frac{P_{max}}{J_{SC} \times V_{OC} \times A} \tag{17}$$

$$P_{light} = 100mW \cdot cm^{-2} \times A \tag{18}$$

$$\eta = \frac{P_{max}}{P_{light}} \times 100\% \tag{19}$$

$$P_{out} = J \times V \times A \tag{20}$$

## 4   Simulation Results

The simulation was run from $d = 200$ nm to $d = 3000$ nm with intervals of 200 nm. Values of $J$, $V$ and output power were calculated for each photoanode thickness as well as for the different absorption coefficients. Relevant graphs were plotted and efficiencies of the DSSCs were determined. Effects of $d$ and $\alpha$ on the performance of simulated ZnO DSSC were discussed.

### 4.1   Effects of Photoanode Thickness

When the simulation is run, a two-dimensional surface plot visualising the distribution of free electron concentration is produced as shown in Fig. 5.

Concentration of free electrons are higher at the electrolyte-photoanode interface, indicated by hotter colours because photogeneration occurs here. Towards the photoanode-TCO interface, free electrons are reduced, as depicted by cooler colours, due to electron recombination.

Table 2 shows the solutions for $J$, $V$ and output power for each $d$. The absorption coefficient used was of ZnO and N719 dye composite found in Table 5. The obtained solutions for $J$, $V$ and output power against $d$ are plotted in Figs. 6 and 7.
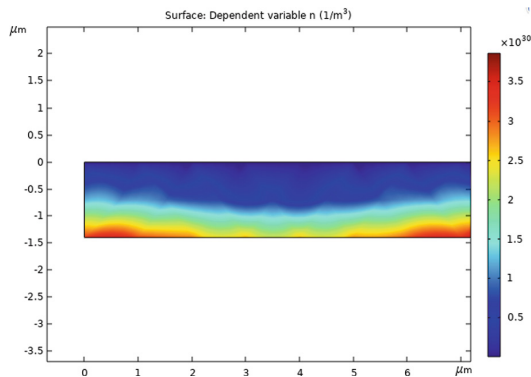
**Fig. 5.** Example of 2D surface plot of distribution of free electron concentration in the photoanode layer.

**Table 2.** *J*, *V* and output power for different photoanode thicknesses

| Thickness, $d$ (nm) | Current density, $J$ (mA/cm$^2$) | Voltage, $V$ (V) | Output power, $P_{out}$ (µW) |
|---|---|---|---|
| 200 | 11.574 | 0.814 | 0.236 |
| 400 | 15.202 | 0.781 | 0.297 |
| 600 | 16.336 | 0.756 | 0.309 |
| 800 | 16.687 | 0.735 | 0.307 |
| 1000 | 16.790 | 0.718 | 0.302 |
| 1200 | 16.755 | 0.704 | 0.295 |
| 1400 | 16.815 | 0.692 | 0.291 |
| 1600 | 16.805 | 0.682 | 0.287 |
| 1800 | 16.792 | 0.673 | 0.283 |
| 2000 | 16.776 | 0.664 | 0.279 |
| 2200 | 16.758 | 0.657 | 0.275 |
| 2400 | 16.739 | 0.650 | 0.272 |
| 2600 | 16.718 | 0.644 | 0.269 |
| 2800 | 16.696 | 0.638 | 0.267 |
| 3000 | 16.672 | 0.633 | 0.264 |

Figure 6 shows *J* increasing with increasing *d* until reaching the maximum at 1400 nm, then reducing again. This conforms with other research results using both fabricated and simulated DSSC. On the other hand, *V* steadily decreases due to increasing series internal resistance caused by thicker photoanode layer [6][15][17]. The value of *J* is high compared to other simulation studies. Studies using TiO$_2$ nanoparticle based DSSC obtained 11.3 mA/cm$^2$ for an optimum thickness of 24 µm [19] and 2.885 mA/cm$^2$ for
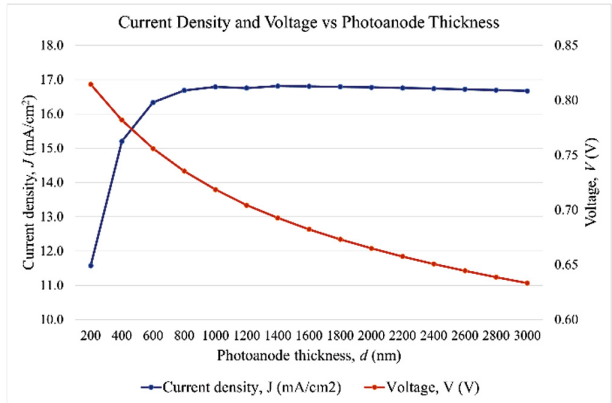
**Fig. 6.** Graph of $J$ and $V$ against $d$ for N719 dye.

**Table 3.** Performance parameters of DSSC with N719 dye

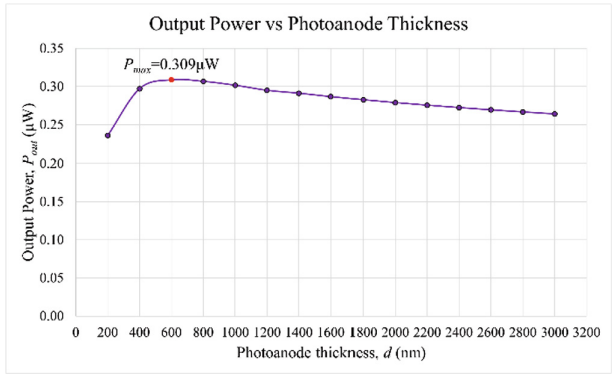| $J_{maxp}$ (mA/cm$^2$) | $V_{maxp}$ (V) | $P_{max}$ (μW) | $J_{SC}$ (mA/cm$^2$) | $V_{OC}$ (V) | $FF$ | $\eta$ (%) |
|---|---|---|---|---|---|---|
| 16.336 | 0.756 | 0.309 | 16.790 | 0.83 | 0.887 | 12.4 |



**Fig. 7.** Output power for different $d$ for N719 dye.

an optimum thickness of 11 μm [24]. These values of $J$ are lower than the 16.8153 mA/cm$^2$ obtained in this simulation at 1400 nm, although their photoanode thicknesses are much larger. High $J$ is attributed to longer electron lifetime and diffusion length. On the other hand, range of $V$ conforms with literature review, which is close to 1 V [9][19].

Optimum thickness is chosen as the thickness at which output power is maximum. In Fig. 7, the output power increases until optimum thickness is reached at 600 nm and decreases again as expected. However, literature review on other TiO$_2$ based DSSC simulation, optimum thickness occurs at around 10 μm to 20 μm [1][15][19]. The minimum recorded was 5 μm [20], below which electron diffusion did not happen
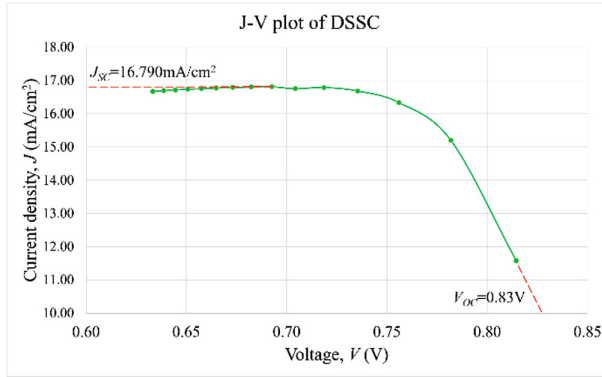
**Fig. 8.** *J-V* plot of simulated DSSC with N719 dye.

optimally. This could translate to low manufacturing cost of mesoporous ZnO-based DSSC due to less amount of material being needed for the best performance. Optimum photoanode thickness achieved by fabricated ZnO DSSC using synthetic dye was as small as 5 nm [9] according to literature review. Fabricated TiO$_2$ DSSC is also able to produce maximum *J* at 292 nm [2].

Figure 8 shows the *J-V* plot of the simulated DSSC with N719 dye. The shape of the curve is as expected from literature review. The 'squareness' of the *J-V* plot can be described by *FF* [6][5][10][19][23]. *FF* is a measure of how close a solar cell is to an ideal source having zero internal resistance.

The performance parameters of the DSSC are summarised in Table 3. $J_{SC}$ and $V_{OC}$ were determined by extrapolating the *J-V* plot. $P_{max}$ is lower than simulated and fabricated values for TiO$_2$ reported, which are 1.008 μW [2] and 0.03 mW [1], respectively. However, this is due to the area of DSSC used in this simulation being smaller compared to ones used in the aforementioned studies. Larger surface area of DSSC harvests more light energy, giving greater current density. A more fitting comparison would be efficiency, which defines the fraction of collected power that can actually be used to do work. DSSC with $\eta$ of 12.4% is high compared to other simulated ones that range between 2% to 5% [1][19][20][23][24]. The *FF* obtained in this work, 0.887, is very high and close to one, indicating very low internal resistance.

The good performance of DSSC in this work could be a result of certain electrical properties of mesoporous ZnO which are more favourable than TiO$_2$. Table 4 shows several electrical properties of mesoporous TiO$_2$. Compared to the corresponding electrical properties of mesoporous ZnO in Table 1, although diffusion coefficient of TiO$_2$ is greater, the long electron lifetime and lower ideality factor of ZnO results in lower recombination rate.

### 4.2 Effects of Absorption Coefficient

Table 5 shows the composite absorption coefficients of ZnO sensitised with different dyes, calculated using Eqs. (7) and (8) from various references, where absorption coefficient of ZnO, $\alpha_2$ is 15957 cm$^{-1}$ [31]. Optimum *d* of 600 nm is used. The corresponding

**Table 4.** Electrical properties of mesoporous $TiO_2$

| Electrical Properties | Mesoporous $TiO_2$ |
|---|---|
| Diffusion coefficient, $D_0$ | $5 \times 10\text{–}4 \ cm^2s^{-1}$ [5] |
| Electron lifetime, $\tau_0$ | 0.04 s [30] |
| Ideality factor, $\gamma$ | 4.5 [5] |

**Table 5.** Absorption coefficient of different dyes and composite absorption coefficients of ZnO sensitised with those dyes

| Dye | Absorption coefficient of dye, $\alpha_1$ $(cm^{-1})$ | Ref. | Composite absorption coefficient, $\alpha$ $(cm^{-1})$ |
|---|---|---|---|
| N719 | 42 000 | [32] | 57 957 |
| Betalain | 37 006 | [33] | 52 963 |
| Chlorophyll | 28 782 | [34] | 44 739 |
| Anthocyanin | 26 661 | [35] | 42 618 |

$J$, $V$, output power and efficiency are tabulated in Table 6. Output power and efficiencies are calculated as shown in Eq. (21) and Eq. (22).

$$P_{out} = J \times V \times A \tag{21}$$

$$\eta = \frac{P_{out}}{P_{light}} \times 100\% \tag{22}$$

Figure 9 shows $J$ increasing as composite absorption coefficient increases, which conforms with other simulation works [5][20][25]. As theorised, higher absorption coefficient causes more light to be absorbed by the photoanode layer, thus increasing the number of photogenerated electrons.

Figure 10 shows the trend of $\eta$ increasing with composite absorption coefficient. This is linked to higher ratio of output power to input power. More of the incident light power are able to be converted into electrical power. From the natural dyes studied, betalain has the highest absorption coefficient and results in greatest efficiency. Table 6 shows that the performance of DSSC does not vary greatly between the distinct dyes. However, this is only for a small area of the solar cell. When manufactured as a panel with a wide area of multiple cells, even small differences will be amplified and greatly affect overall performance. Besides that, absorption coefficient is not the only factor to be accounted for. Acidity and recombination property of dyes also play an important part. For example, N719 dye is known to cause breakdown of mesoporous ZnO photoanode into $Zn^{2+}$ ions [16] which inhibits electron injection. Although $\alpha_1$ is smaller for the natural dyes, their neutral pH works better with ZnO. Ultimately this may result in natural dyes procuring higher efficiencies for ZnO-based DSSC.
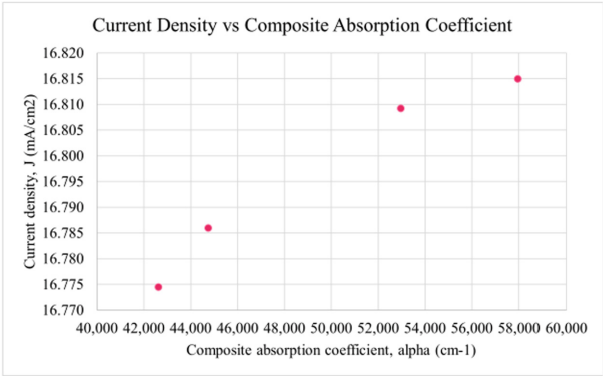
**Fig. 9.** Graph of $J$ against $\alpha$ for $d = 600$ nm.

**Table 6.** $J$, $V$, output power and efficiencies of DSSC using dyes of different absorption coefficients for $d = 600$ nm

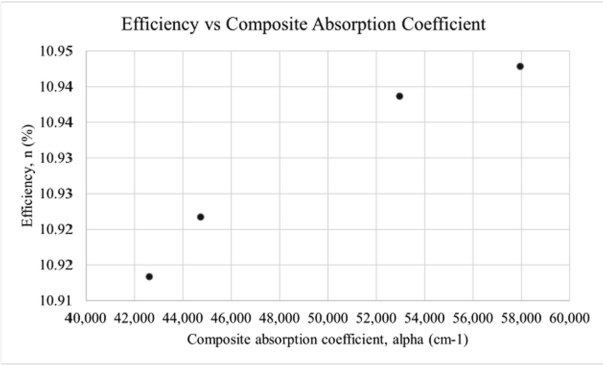| Dye | Composite absorption coefficient, $\alpha$ (cm$^{-1}$) | Current density, $J$ (mA/cm$^2$) | Voltage, $V$ (V) | Output power, $P_{out}$ ($\mu$W) | Efficiency, $\eta$ (%) |
|---|---|---|---|---|---|
| N719 | 57 957 | 16.8150 | 0.6508 | 0.2736 | 10.94 |
| Betalain | 52 963 | 16.8093 | 0.6508 | 0.2735 | 10.94 |
| Chlorophyll | 44 739 | 16.7860 | 0.6506 | 0.2730 | 10.92 |
| Anthocyanin | 42 618 | 16.7745 | 0.6506 | 0.2728 | 10.91 |



**Fig. 10.** Graph of $\eta$ against $\alpha$ for $d = 600$ nm.

## 5  Conclusion

The numerical simulation of ZnO based DSSC was successful in proving that meso-porous ZnO is able to compete with TiO$_2$ in producing high-efficiency DSSCs. The optimum range of thickness for mesoporous ZnO DSSC is between 400 nm to 1200 nm as it results in high output power compared to other photoanode thicknesses. From the natural dyes tested, betalain procured the greatest efficiency for photoanode thickness within the optimum range. The best combination of materials from this study is a ZnO DSSC of 600 nm thickness, sensitised with betalain. Efficiency can be further increased to compete with synthetic dyes by introducing other factors such as doping.

This project can be extended to include internal resistance and reverse saturation current density for better results. The present model considers only a single cell while in practice, there are other important components, such as the TCO and interconnections, which cause internal serial resistance to the flow of electrons. Other than that, optimum thickness determined from N719 dye might not be the same for other dyes. Depending on the absorption coefficient of dyes, optimum thickness might be different due to different absorption spectrum covered by the dyes. Parametric sweep of photoanode thickness for each of the dyes can be the next step in improving this study. Numerical models of DSSC can be further improved to include favourable properties of natural dyes since they have been proven better than synthetic dyes in certain conditions but unable to be characterised as such by simulated DSSCs.

**Authors' Contributions.**  *Conceptualization:* P. L. Low, M. E. Yeoh and K. Y. Chan; *data acquisition:* L. Arumugam; *formal analysis:* L. Arumugam, P. L. Low, and Y. K. Sin; *writing original draft:* L. Arumugam; *review and editing:* L. Arumugam, P. L. Low and G. Thien; *supervision and project administration:* P. L. Low, Y. K. Sin and K. Y. Chan.

## References

1. A. Baarar, M. Vlaadescu, and P. Schiopu, Influence of TiO2 Layer Thickness on The Performance of Dye-Sensitized Solar Cells: Theoretical Investigations, in: 2020 IEEE 8th Electronics System-Integration Technology Conference *(ESTC)*, 2020. DOI: https://doi.org/10.1109/ESTC48849.2020.9229790

2. S. H. Pramono, E. Maulana, and M. A. R. Sembiring, The Effect of Photo electrode TiO2 Layer Thickness to The Output Power of Chlorophyll-Based Dye-Sensitized Solar Cell (DSSC), in: 2015 International Seminar on Intelligent Technology and Its Applications (ISITIA), 2015. DOI: https://doi.org/10.1109/ISITIA.2015.7219963

3. D. Goswami, D. Sinha, and D. De, Nanostructured ZnO and Natural Dye Based DSSC for Efficiency Enhancement, in: 2017 Third International Conference on Science Technology Engineering & Management (ICONSTEM), 2017. DOI: https://doi.org/10.1109/ICONSTEM.2017.8261430

4. T. Bhavani K, D. N. Joshi, and V. Dutta, Tandem DSSC fabrication by controlled infiltration of organic dyes in mesoporous electrode using electric-field assisted spray technique, in: Solar Energy, vol. 223, 2021, pp. 318–325. DOI: https://doi.org/10.1016/j.solener.2021.05.060

5. A. Aboulouard, S. Rbihi, Y. Najih, M. Adar, A. Jouaiti, B. Elhadadi, and M. A. El Abbassi, Numerical Simulation of Dye-Sensitized Solar Cells Performance for Local Natural Dyes, in: 2020 IEEE 6th International Conference on Optimization and Applications (ICOA), 2020. DOI: https://doi.org/10.1109/ICOA49421.2020.9094508

6. M. Wright and A. Uddin, Organic—inorganic hybrid solar cells: A comparative review, in: Solar Energy Materials and Solar Cells, vol. 107, Sep. 2012, pp. 87–111. DOI: http://dx.doi.org/10.1016/j.solmat.2012.07.006

7. J. Maçaira, L. Andrade, and A. Mendes, Modeling, simulation and design of dye sensitized solar cells, in: RSC Adv., vol. 4, no. 6, 2014, pp. 2830–2844. DOI: https://doi.org/10.1039/C3RA46295A

8. S. Singh, A. Singh, and N. Kaur, Efficiency investigations of organic/inorganic hybrid zno nanoparticles based dye-sensitized solar cells, in: Journal of Materials, vol. 2016, 2016, pp. 1–11. DOI: https://doi.org/10.1155/2016/9081346

9. A. K. Chandiran, M. Abdi-Jalebi, M. K. Nazeeruddin, and M. Grätzel, Analysis of electron transfer properties of zno and tio2 Photoanodes for dye-sensitized solar cells, in: ACS Nano, vol. 8, no. 3, 2014, pp. 2261–2268. DOI: https://doi.org/10.1021/nn405535j

10. S. C. Ramesh, P. Ramkumar, C. C. Columbus, and X. S. Shajan, Experimental and simulation studies of platinum-free counter electrode material for Titania aerogel-based quasi-solid dye-sensitized solar cell, in: IEEE Journal of Photovoltaics, vol. 10, no. 6, 2020, pp. 1757–1761. DOI: https://doi.org/10.1109/JPHOTOV.2020.3025693

11. N. Jamalullail, I. S. Mohamad, M. N. Norizan, N. A. Baharum, and N. Mahmed, Short review: Natural pigments photosensitizer for dye-sensitized solar cell (DSSC), in: 2017 IEEE 15th Student Conference on Research and Development (SCOReD), 2017. DOI: https://doi.org/10.1109/SCORED.2017.8305367

12. A. N. Ossai, A. B. Alabi, S. C. Ezike, and A. O. Aina, Zinc oxide-based dye-sensitized solar cells using natural and synthetic sensitizers, in: Current Research in Green and Sustainable Chemistry, vol. 3, 2020, p. 100043. DOI: https://doi.org/10.1016/j.crgsc.2020.100043

13. S. I. Cho, H. K. Sung, S.-J. Lee, W. H. Kim, D.-H. Kim, and Y. S. Han, Photovoltaic performance of dye-sensitized solar cells containing zno microrods, in: Nanomaterials, vol. 9, no. 12, 2019, p. 1645. DOI: https://doi.org/10.3390/nano9121645

14. R. Chang, K. Ithisuphalap, and I. Kretzschmar, Impact of particle shape on electron transport and lifetime in zinc oxide nanorod-based dye-sensitized solar cells, in: AIMS Materials Science, vol. 3, no. 1, Jan. 2016, pp. 51–65. DOI: http://dx.doi.org/10.3934/matersci.2016.1.51

15. W.-C. Chang, C.-H. Lee, W.-C. Yu, and C.-M. Lin, Optimization of dye adsorption time and film thickness for efficient zno dye-sensitized solar cells with high at-rest stability, in: Nanoscale Research Letters, vol. 7, no. 1, Dec. 2012, p. 688. DOI: https://doi.org/10.1186/1556-276X-7-688

16. K. Keis, J. Lindgren, S.-E. Lindquist, and A. Hagfeldt, Studies of the adsorption process of RU complexes in nanoporous zno electrodes, in: Langmuir, vol. 16, no. 10, 2000, pp. 4688–4694. DOI: https://doi.org/10.1021/la9912702

17. X. Sheng, Y. Zhao, J. Zhai, L. Jiang, and D. Zhu, Quasi-solid-state dye-sensitized solar cells based on zno photoanode, in: Chemical Engineering Communications, vol. 195, no. 4, 2007, pp. 375–385. DOI: https://doi.org/10.1080/00986440701709426

18. T. Hatem, Z. Ismail, M. G. Elmhgary, R. Ghannam, M. A. Ahmed, and S. O. Abdellatif, Optimization of organic meso-superstructured solar cells for underwater IOT2 self-powered sensors, in: IEEE Transactions on Electron Devices, vol 68, no. 10, 2021, pp. 5319–5321. DOI: http://dx.doi.org/10.1109/TED.2021.3101780

19. S. C. Ramesh, C. C. Columbus, and X. S. Shajan, Modeling and simulation of a dye sensitized solar cell with porous aerogel photoanode, in: Journal of Electrical Engineering & Technology, vol. 16, no. 1, 2021, pp. 509–514. DOI: https://doi.org/10.1007/s42835-020-00600-9

20. M. Ni, M. K. Leung, and D. Y. Leung, Theoretical modelling of the electrode thickness effect on maximum power point of dye-sensitized solar cell, in: The Canadian Journal of Chemical Engineering, vol. 86, no. 1, Mar. 2008, pp. 35–42. DOI: http://dx.doi.org/10.100/Fcjce.20015

21. A. A. E. Tayyan, DYE SENSITIZED SOLAR CELL: PARAMETERS CALCULATION AND MODEL INTEGRATION, in: Journal of Electron Devices, vol. 11, 2011, pp. 616–624.

22. P. Guo, S. Q. Li, N. Zhou, J. Zhang, and R. P. H. Chang, Optical and Electrical Modeling of Three Dimensional Dye-Sensitized Solar Cells, in: COMSOL Conference, Boston, 2013.

23. M. Mehrabian and S. Dalir, Numerical simulation of highly efficient dye sensitized solar cell by replacing the liquid electrolyte with a semiconductor solid layer, in: Optik, vol. 169, 2018, pp. 214–223. DOI: http://dx.doi.org/10.1016/j.ijleo.2018.05.059

24. S. Manouchehri, J. Zahmatkesh, and M. H. Yousefi, Two-dimensional optical fiber-based dye-sensitized solar cell simulation: The effect of different electrodes and dyes, in: Journal of Computational Electronics, vol. 17, no. 1, 2017, pp. 329–336. DOI: https://doi.org/10.1007/s10825-017-1076-6

25. M. Bavarian, S. Nejati, K. K. Lau, D. Lee, and M. Soroush, Theoretical and experimental study of a dye-sensitized solar cell, in: Industrial & Engineering Chemistry Research, vol. 53, no. 13, 2013, pp. 5234–5247. DOI: https://doi.org/10.1021/ie4016914

26. Theory, in: Beer-Lambert's law for multicomponent system (Theory): Absorption spectroscopy: Biotechnology and Biomedical Engineering: Amrita Vishwa Vidyapeetham Virtual Lab. [Online]. Available: https://vlab.amrita.edu/?sub=3&brch=206&sim=579&cnt=1.

27. A. P. Uthirakumar, Fabrication of zno based dye sensitized solar cells, in: Solar Cells - Dye-Sensitized Devices, 2011. DOI: http://dx.doi.org/10.5772/19459

28. P. Tiwana, P. Docampo, M. B. Johnston, H. J. Snaith, and L. M. Herz, Electron mobility and injection dynamics in mesoporous zno, Sno2, and tio2 films used in dye-sensitized solar cells, in: ACS Nano, vol. 5, no. 6, 2011, pp. 5158–5166. DOI: https://doi.org/10.1021/nn201243y

29. T.-H. Lee, H.-J. Sue, and X. Cheng, Solid-state dye-sensitized solar cells based on zno nanoparticle and nanorod array hybrid photoanodes, in: Nanoscale Research Letters, vol. 6, no. 1, 2011. DOI: https://doi.org/10.1186/1556-276X-6-517

30. K. Park, Q. Zhang, D. Myers, and G. Cao, Charge transport properties in tio2 network with different particle sizes for dye sensitized solar cells, in: ACS Applied Materials & Interfaces, vol. 5, no. 3, 2013, pp. 1044–1052. DOI: https://doi.org/10.1021/am302781b

31. H. S. Bolarinwa, M. U. Onuu, A. Y. Fasasi, S. O. Alayande, L. O. Animasahun, I. O. Abdulsalami, O. G. Fadodun, and I. A. Egunjobi, Determination of optical parameters of zinc oxide nanofibre deposited by electrospinning technique, in: Journal of Taibah University for Science, vol. 11, no. 6, 2017, pp. 1245–1258. DOI: https://doi.org/10.1016/j.jtusci.2017.01.004

32. Y. Sun, A. C. Onicha, M. Myahkostupov, and F. N. Castellano, Viable alternative to N719 for dye-sensitized solar cells, in: ACS Applied Materials & Interfaces, vol. 2, no. 7, 2010, pp. 2039–2045. DOI: https://doi.org/10.1021/am100311m

33. K. U. Isah, B. J. Jolayemi, U. Ahmadu, M. I. Kimpa, and N. Alu, Plasmonic effect of silver nanoparticles intercalated into mesoporous betalain-sensitized-tio2 film electrodes on photovoltaic performance of dye-sensitized solar cells, in: Materials for Renewable and Sustainable Energy, vol. 5, no. 3, 2016. DOI: https://doi.org/10.1007/s40243-016-0075-z

34. C. Cari, Khairuddin, T. Y. Septiawan, P. M. Suciatmoko, D. Kurniawan, and A. Supriyanto, The preparation of natural dye for dye-sensitized solar cell (DSSC), in: AIP Conference Proceedings, 2018. DOI: https://doi.org/10.1063/1.5054510

35. M. Hosseinnezhad, S. Moradian, and K. Gharanjig, Fruit extract dyes as photosensitizers in solar cells, in: Current Science, vol. 109, no. 5, 2015, p. 953. DOI: https://doi.org/10.18520/v109/i5/953-956